Physicochem. Probl. Miner. Process., 61(5), 2025, 210998

http://www.journalssystem.com/ppmp

Physicochemical Problems of Mineral Processing

ISSN 1643-1049

Mechanism of a combined depressant of Fe^{3+} and corn starch on the flotation separation of magnetite and quartz

Qian Wang [1], Dong Wang [2], Quanxiang Yan [3]

[1] Shandong Key Laboratory of Intelligent Magnetoelectric Equipment and Mineral Processing Technology, Weifang, 262600, China

[2] School of Materials Science and Engineering, Fuzhou University, Fuzhou 350116, China

[3] Zijin School of Geology and Mining, Fuzhou University, Fuzhou, 350116, Fujian, China

Corresponding author: dongwang20221993@163.com (Dong Wang), yanlady@163.com (Quanxiang Yan)

Abstract: The effective separation of magnetite (Fe_3O_4) and quartz (SiO_2) is essential for mineral purification in the field of mineral resource utilization. In this study, we examined the effects of Fe^{3+} and corn starch (CS) on the flotation separation of magnetite and quartz using micro-flotation experiments, solution chemistry calculations, Fourier transform infrared spectroscopy (FT-IR), zeta potential tests, contact angle tests, and scanning electron microscopy (SEM). The results of our micro-flotation experiment demonstrated that the combined depressant of CS and Fe^{3+} significantly depressed the flotation of magnetite. When the pH value was 10, the CS concentration was 8 mg/l, the Fe^{3+} concentration was 150 mg/l and the dodecamine concentration was 6 mg/l; approximately 19.30% of the magnetite and 72.01% of the quartz entered the foam product. In addition, the results of SEM and FT-IR analyses revealed that the addition of Fe^{3+} significantly enhanced the selective depressant effect of CS on magnetite. This effect was the result of Fe^{3+} undergoing hydrolysis reactions on the surface of magnetite, forming $Fe(OH)_3$ and $Fe(OH)_2$ precipitates, which both enhance the binding strength between CS and the mineral surface through chemical adsorption. Lastly, the zeta potential and contact angle test results further revealed that Fe^{3+} alters the charge distribution on the magnetite surface, reduces the absolute value of the potential, and weakens its surface hydrophobicity.

Keywords: magnetite, quartz, reverse flotation separation, Fe^{3+} and CS as depressants

1. Introduction

Iron ore is a strategic key raw material for China's steel industry and is related to national economic security. It not only serves as an important raw material for steel production but is also widely utilized in powder metallurgy, material processing, machinery manufacturing, energy processing, transportation, and other important fields (Yang et al., 2019; Yang et al., 2018; Zhang et al., 2017; Luo et al., 2021; Luo et al., 2016). In magnetite ore, quartz and feldspar are common silicate gangue minerals, and they are generally embedded in ore deposits formed by rock fractures or gangue structures (Chang et al., 2022; Guang et al., 2019). Although magnetite and quartz share some similarities in their physical and chemical properties (such as thermal stability and corrosion resistance), there is a significant difference in their densities, making separation difficult. In order to achieve efficient separation of magnetite and quartz by flotation, an effective depressant is still needed.

With growing environmental awareness, organic depressants are gradually gaining increasing attention due to their widespread availability, low cost, and environmentally friendly characteristics. Desilification is of great significance for improving the grade of iron ore concentrate, as excessive quartz severely limits the utilization efficiency of iron ore (Zhan et al., 2023). Recent studies have shown that although amine collectors are widely used in the separation of magnetite and quartz, there are still problems such as high reagent consumption and poor selectivity (Zhan et al., 2013). In the process of flotation separation and purification of minerals, organic depressants are not only used to reduce negative environmental impacts but also to reduce dependence on traditional chemicals. Among the

DOI: 10.37190/ppmp/210998

various organic depressants available, hydroxypropyl methylcellulose, pectin, and glucose are particularly common (Shen et al., 2023; Wang et al., 2023; Qiu et al., 2018; Li et al., 2019). Ammar et al. (Ammar et al., 2022) investigated two hydrolytic enzymes as flotation separation depressants for apatite and hematite. Their experimental results demonstrated that when pH = 10, the adsorption strength and selectivity of the hydrolytic enzyme on hematite are superior to the iron recovery rate obtained when starch is used at pH = 10.5. In addition, Yehia et al. (Yehia et al., 2021) focused on using fungal cellulase in their study to selectively separate hematite and apatite. The results demonstrated that the hydrophobicity of the apatite surface must be greater than the adsorption effect of cellulase, which is crucial for depressing hematite flotation. It is worth noting that the abovementioned depressants are all high-molecular-weight organic compounds. Due to their poor solubility, the industrial application of organic compounds is significantly restricted.

In recent years, during the processing of specific complex iron ores, particularly those that are difficult to selectively depress using standard methods, it is usually necessary to use large amounts of regular starch. However, the depressant effect is not efficient (Rocha et al., 2019; Oulkhir et al., 2025; Oulkhir et al., 2025, Oulkhir et al., 2025a; Oulkhir et al., 2025b; Hong et al., 2025). With the aim of improving the efficiency of mineral depressants, a number of scholars have shifted their research focus to studying the synergistic application of metal ions and starch (Yehia et al., 2021; Rath et al., 2022; Tang et al., 2019; Cai et al., 2022). Several studies have been conducted on the interaction mechanism of metal ions and flotation reagents. The results of such studies demonstrate that selective pre-adsorption on the mineral surface can alter the surface's chemical composition and subsequently create more active sites for subsequent flotation reagent adsorption (Zhao et al., 2019; de et al., 2023). Extensive evidence indicates that Ca^{2+}, K^{+}, Mg^{2+}, Na^{+}, and other metal ions, acting as activators, can improve the flotation separation of magnetite and quartz (Gao et al., 2021; Gao et al., 2021, Gao et al., 2021a; Gao et al., 2021b). However, Fe^{2+} and Al^{3+}, acting as depressants, are readily adsorbed onto the surface of siliceous gangue minerals, such as quartz. Metal ions therefore make the flotation process more complex and the separation process more difficult (Gao et al., 2021a; Gao et al., 202b1; Gao et al., 2021; Jie et al., 2014; Tang et al., 2020). Thus far, there have been very few domestic and international studies on the effects of Fe^{3+} on the flotation separation behavior of quartz and magnetite. An in-depth examination of the behavior of Fe^{3+} and CS combined depressant during the flotation separation of quartz and magnetite is therefore of great theoretical and practical importance. Evidence demonstrates that Fe^{3+} and CS alter mineral surface properties and determine flotation behavior. The above references provide us with new insights into the comprehensive utilization of iron ore.

Magnetite and quartz share certain similarities in terms of chemical properties (such as corrosion resistance and electrical conductivity), but there are still differences in their overall physical and chemical properties, making separation difficult. In addition, the effectiveness, selectivity, and operability of a single starch depressant still require further optimization. To overcome these constraints, we propose the use of CS and Fe^{3+} as a combined depressant strategy. By regulating the hydrolysis process of Fe^{3+} ions in the slurry and the formation of $Fe(OH)_3$ and $Fe(OH)_2$ precipitates on the mineral surface, this strategy significantly enhances the selective adsorption ability of starch on magnetite, with Fe^{3+} having a relatively minor effect on quartz. To validate the effectiveness of the combined depressant mechanism, we systematically analyzed the effects of CS and Fe^{3+} on the flotation separation of magnetite and quartz using a variety of technical methods, including flotation experiments, solution chemistry calculations, Fourier transform infrared spectroscopy (FT-IR) analysis, zeta potential testing, and contact angle measurement. Lastly, we conduct a detailed analysis of the adsorption properties of CS and Fe^{3+} on mineral surfaces, determine the underlying mechanisms of magnetite and quartz flotation separation, and provide an innovative technical approach for the highly efficient and environmentally friendly separation of magnetite and quartz. The research findings also offer valuable insights into the development of depressants in the field of mineral processing.

2. Materials and methods

2.1. Materials and reagents

The magnetite and quartz samples used in this study were collected from Baoshan, Yunnan Province, China. The original ore samples were crushed to less than 2 mm using a small double-roll crusher;

thereafter, impurities were manually removed from the samples under an optical microscope. A three-head grinding machine (model XPM-φ120×3, Ganzhou, China) was used in the grinding process to obtain powder samples with a fineness of less than 200 mesh for experiments and analysis. The X-ray diffraction analysis results of magnetite and quartz are shown in Fig. 1. As can be seen from the Fig.s below, the samples are pure minerals and can be used for further analysis.

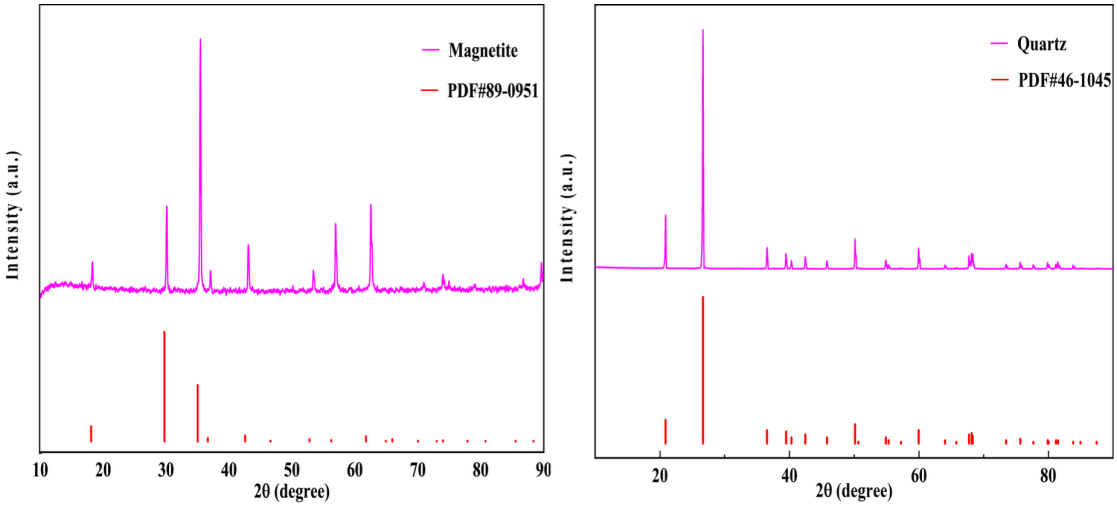

Fig. 1. (a) XRD pattern of the pure magnetite mineral sample and (b) XRD pattern of the pure quartz mineral sample

2.2. Reverse micro-flotation tests

Pure mineral flotation tests were carried out using an XFGC pneumatic hanging tank flotation machine at room temperature. The air flow rate was set at 16 cm^3/min, and the impeller speed was set at 1600 rpm. The procedure required for the micro-flotation test was as follows: (a) A flotation tank was filled with 30 mL deionized water and artificial samples composed of 1 g magnetite and 1 g quartz. Next, the flotation slurry was stirred at a rate of 1500 rpm for two minutes. (b) The pulp pH was adjusted using hydrochloric acid and sodium hydroxide as pH regulators, maintaining stability within the range of pH = 7 to 12 set in this experiment, and agitated for one minute. (c) Thereafter, starch was added, and the mixture was agitated for a further two minutes, after which metal ions were added and left for two minutes. (d) The dodecylamine(DDA) was added at a concentration of 6 mg/l, and the mixture was aerated for three minutes before automatic bubble scraping was performed. The concentration and tailings were collected, filtered, dried, and weighed to determine the flotation recovery. The ε (%) for the flotation recovery of single and mixed minerals was calculated using Eq. (1):

$$\varepsilon = \frac{m_1}{m_1+m_2} \times 100\% \tag{1}$$

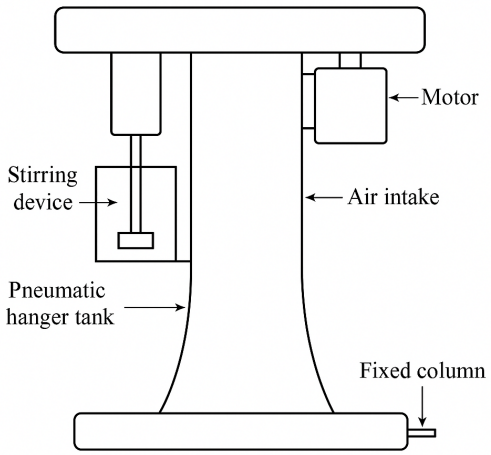

Fig. 2. Schematic diagram of XFGC pneumatic suspension flotation machine

Equation (1) is used to calculate the flotation recovery, where m_1 is the mass of the con-cen-trate and m_2 is the mass of the tailings. The recovery (%) is defined as the proportion of concen-trate mass relative to the total mass of the flotation products. The flotation tests were conducted in triplicate, and the average values were taken.

2.3. Solution chemistry calculations

Visual MINTEQ software (version 3.1) is generally used to calculate how metal ions affect the saturation index (*SI*) of magnetite, quartz, and prospective mineral solutions at various pH levels. The saturation index *SI* can be calculated using Eq. (2) (Benavente et al., 2025):

$$\mathrm{SI} = \log(\mathrm{IAP}/\mathrm{Ks}) \tag{2}$$

where *Ks* is the solubility product and *IAP* is the ion activity product. The saturation index clearly demonstrates how stable a mineral is in a thermodynamic system. When the saturation index $SI > 0$, this indicates that the solid phase is likely to form, and the higher the *SI* value, the stronger the stability of the solid phase and the greater the possibility of the existence of specific potential minerals. The chemical equilibrium of the solution is calculated using Eq. (3) (Henry et al., 2001):

$$\mathrm{pH} = \mathrm{pK} + \log\left([\mathrm{A}^-]/[\mathrm{HA}]\right) \tag{3}$$

Eq. (3) denotes the amount of conjugate base $[A^-]$ and the amount of weak acid [HA], which are closely related to the negative logarithm of the acid dissociation constant *pK* of the weak acid (HA). When the pH of the solution is equal to the *pK* value of the weak acid, the proportions of the conjugate base $[A^-]$ and the weak acid [HA] are equal, indicating that the acid and base in the solution are in dynamic equilibrium.

2.4. FT-IR Spectroscopic characterization

The analysis was performed using a Thermo Fisher Nicolet iS50 Fourier transform infrared spectrometer. The instrument settings were as follows: ten scans, spectral resolution of 4 cm^{-1}, and a spectral scan range of 4000 to 400 cm^{-1} wavenumber interval. The specific procedure is as follows: First, take an appropriate amount of sample and potassium bromide and thoroughly grind and mix them in an agate mortar to ensure that the minerals are evenly dispersed in the potassium bromide matrix. Next, use a tablet press to compress the uniformly ground mixture into tablets. Lastly, place the prepared sample tablets into an infrared spectrometer for detection and analysis.

2.5. Zeta potential measurement

Zeta potential testing was performed using a Zetasizer-3000HS potential meter. The sample preparation process for zeta potential testing is as follows: Pure minerals are ground to a particle size of less than 2 μm using an agate grinder. Next, 0.05 g of the sample is weighed and placed in a beaker; thereafter, 50 mL of 5×10 mol/L potassium chloride electrolyte solution is added. The mixture is stirred for 3 minutes using a stirrer operating at 500 r/min until uniformly mixed. Next, the reagents are added based on the flotation reagent schemes, the pulp in the sample cell is left undisturbed for 3 minutes, an appropriate amount of the upper suspension is added to the sample pool, and the potential is measured. Each sample is measured three times under the same conditions, and the average value is taken as the test result.

2.6. Contact angle measurement

The contact angle was measured using a JY-82 video contact angle meter manufactured by Hebei Chengde Ding sheng Testing Equipment Co., Ltd. First, high-purity raw minerals were selected for slicing. The slices were polished using 2000 M and 5000 M fine sandpaper to ensure that the quartz slice surface was free from oxide film coverage and relatively clean. Second, a contact angle measurement instrument was used to measure the contact angle of the treated quartz slices. Once the three-phase line was constructed, an image capture system with a photosensitive coupling component was used to capture images, which were analyzed and processed using specialized software to determine the size of the contact angle.

2.7. SEM analysis

Scanning electron microscopy (SEM) was used to study the morphology and surface composition of magnetite and quartz. Sample preparation was performed based on the following steps: (a) preparation of raw ore samples; (b) addition of 4 mg/l starch to the samples in the flotation cell and stirring at 400 rpm for two minutes; (c) addition of $FeCl_3$ (6 mg/l) and stirring at 400 rpm for two minutes; and (d) drying of the final mineral samples in a vacuum oven to prepare the samples. The prepared samples were analyzed on a Phenom ProX device at an acceleration voltage of 10 kV.

3. Results and discussion

3.1. Reverse micro-flotation tests

To explore the effect of CS dosage and pH value on the separation efficiency of magnetite and quartz, a systematic experimental study was conducted. As shown in Fig. 3(a), as the dosage of CS increases, the recovery rates of magnetite and quartz show a gradual downward trajectory. When the CS dosage reached 8 mg/l, the difference between the quartz and magnetite recovery rates reached its maximum in the flotation process. The recovery rate of quartz remained at a relatively high rate of 87.86%; in comparison, the recovery rate of magnetite decreased to 34.01%. Following further analysis, the results presented in Fig. 3(b) demonstrate the trend in the flotation recovery rates of the two minerals under different pH conditions (pH range from 7 to 12). The recovery rates of magnetite and quartz increase with rising pH, reaching a peak before beginning to decline. It is worth noting that the greatest difference in the recovery rates of magnetite and quartz appears at a pH value of 10. The results of micro-flotation experiments demonstrated that CS significantly depressed the flotation of magnetite; in comparison, its effect on the flotation of quartz was relatively limited.

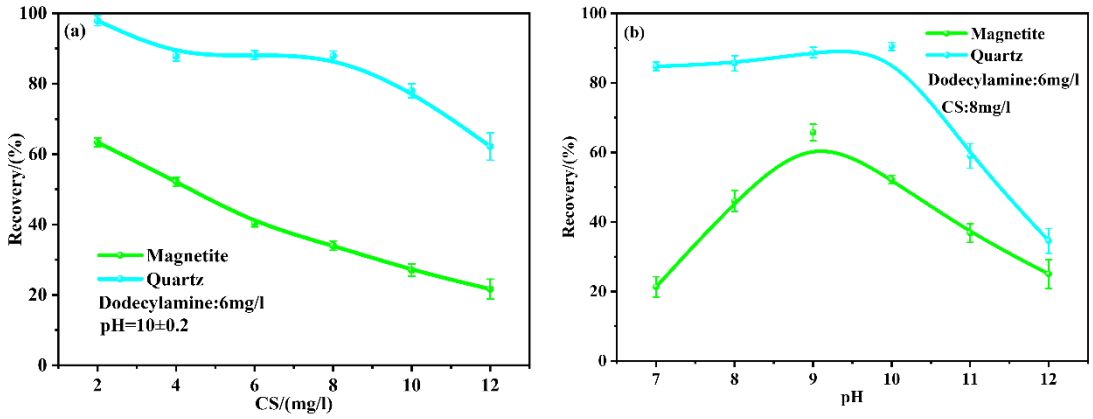

Fig. 3. Effect of (a) the amount of CS and (b) pH on the recovery of magnetite and quartz

The results presented in Fig. 4(a) illustrate the changes in the recovery rates of magnetite and quartz under different Fe^{3+} dosage conditions. With the gradual increase in Fe^{3+} dosage, the recovery rates of minerals exhibit a gradual decreasing trend. This finding may be the result of Fe^{3+} or its hydrolysis products forming a coating layer on the surface of magnetite, which significantly weakens its floatability (Choi et al., 2016). Subsequently, pH value experiments were performed, and the results are presented in Fig. 4(b). The recovery of magnetite and quartz increase up to pH 10 and then decrease thereafter. At a pH value of 10, the recovery rate of quartz exhibited a significant rising inflection point, improving the flotation separation effect of the two minerals.

3.2. Solution chemistry calculations

Visual MINTEQ software includes a broad range of applications that can be used to calculate the distribution of Fe^{3+} species, dissolution equilibrium states, and adsorption phenomena (Tang et al., 2019; Ruan et al., 2018; Chen et al., 2018; Yuan et al., 2025). This analysis tool can accurately calculate the existence form of hydrolysis components or chemical reagents under specific pH conditions and their potential reaction mechanisms. The results presented in Fig. 5 demonstrate the effect of pH changes

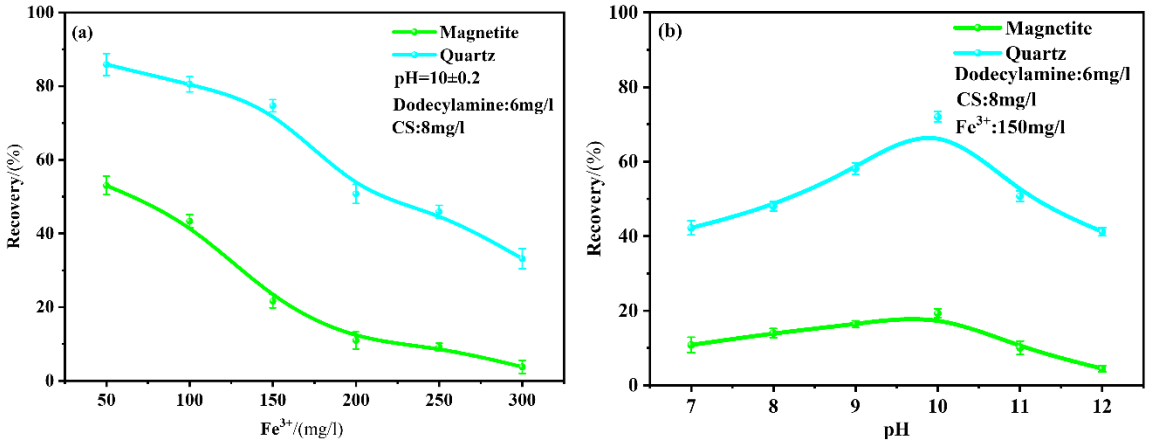

Fig. 4. Effects of (a) the amount of ferric chloride and (b) pH on the recovery of magnetite and quartz

on the Fe^{3+} form and its distribution fractions in the quartz–magnetite solution system. At a pH value of 10, the distribution fractions of Fe^{3+} species follow the decreasing order: $Fe(OH)_4^-$ > $Fe(OH)_2^+$ > $Fe(OH)_2^+$ ~ $Fe(OH)_2^{4+}$ ~ $Fe_3(OH)_4^{5+}$. Under these conditions, ferric components dominate, with $Fe(OH)_4^-$ being the main component in the solution, the distribution fractions of which is significantly higher than that of the other ferric components.

$$Fe^{3+} + OH^- \leftrightharpoons Fe(OH)^{2+} \quad (4)$$

$$Fe^{3+} + 2OH^- \leftrightharpoons Fe(OH)_2^+ \quad (5)$$

$$3Fe^{3+} + 4OH^- \leftrightharpoons Fe_3(OH)_4^{5+} \quad (6)$$

$$Fe^{3+} + 4OH^- \leftrightharpoons Fe(OH)_4^- \quad (7)$$

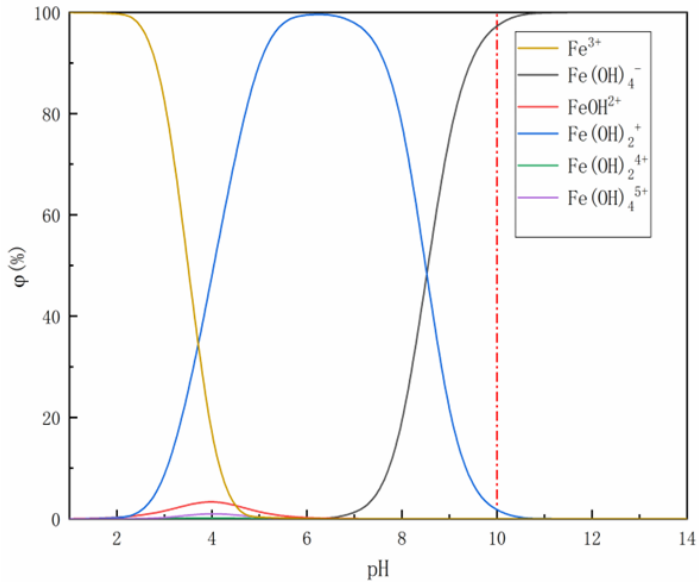

Fig. 5. The effect of pH on Fe^{3+} solution composition in a quartz and magnetite solution system

The results presented in Fig. 6 demonstrate the effect of pH on the saturation index (SI) of potential minerals in a solution system of magnetite and quartz. $Fe(OH)_{3(s)}$, $Fe(OH)_2$, and Fe_2O_3 are minerals that interact with reagents to reach saturation. As the pH value gradually increases, the SI values of these minerals all show an increasing trend and reach their maximum values at specific pH values: that for $Fe(OH)_{3(s)}$ is 15.805, that for $Fe(OH)_2$ is 11.549, and that for Fe_2O_3 is 31.106. As the pH value continues to rise, the SI values of these minerals exhibit a decreasing trend. At a pH value of 10, the SI values of $Fe(OH)_{3(s)}$, $Fe(OH)_2$, and Fe_2O_3 are 14.329, 10.612, and 29.232, respectively. These data demonstrate that the presence of Fe^{3+} significantly depresses the dissolution process of minerals, thereby promoting the

precipitation of $Fe(OH)_{3(s)}$, $Fe(OH)_2$, and Fe_2O_3 on the surfaces of quartz and magnetite. In summary, the adsorption of Fe^{3+} on the mineral surface not only promotes the formation of $Fe(OH)_{3(s)}$, $Fe(OH)_2$, and Fe_2O_3 but also further enhances the depressant effect of CS on magnetite flotation.

$$Fe^{2+} + 2OH^- \leftrightharpoons Fe(OH)_2 \quad (8)$$

$$Fe^{3+} + 3OH^- \leftrightharpoons Fe(OH)_{3\,(s)} \quad (9)$$

$$Fe(OH)_3 + OH^- \leftrightharpoons FeO_2^- + 2H_2O \quad (10)$$

$$2FeO_2^- + 2H_2O \leftrightharpoons Fe_2O_3 + 4OH^- \quad (11)$$

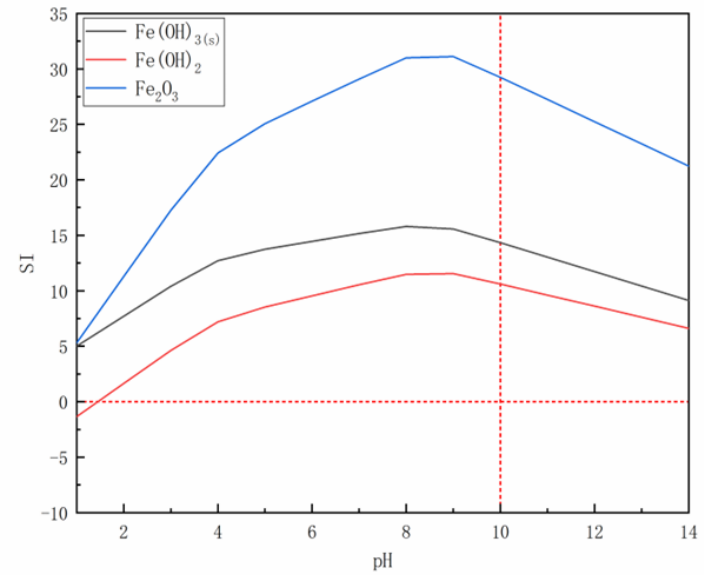

Fig. 6. The saturation index (SI) of potential iron minerals in a quartz and magnetite solution system

3.3. Fourier transform infrared spectrometer (FT-IR)

We aimed to explore the adsorption behavior of CS and Fe^{3+} as depressants on mineral surfaces and their effects on the flotation characteristics of magnetite and quartz samples. The results presented in Fig. 7 illustrate the characteristic peaks of the CS infrared spectrum, which agree with those found in earlier studies. The three peaks at 3426.41, 2929.24, and 1054.25 cm^{-1} correspond to the -OH, -CH2-, and C-OH stretching vibration absorption peaks, respectively (Chen et al., 2020). When dodecylamine, CS, and quartz interact, the absorption peak of the quartz hydroxyl stretching vibration changes significantly in both position and intensity. It is evident that CS has been successfully adsorbed onto the quartz surface by the newly added absorption peak at 2932.32 cm^{-1} in the quartz's infrared spectra, which corresponds to the symmetric stretching vibration of $-CH_2$ (Liu et al., 2011). However, when quartz reacts with Fe^{3+}, CS, and dodecylamine, the intensity of the -OH stretching vibration absorption peak in its infrared spectrum weakens; in comparison, the $-CH_2$ symmetric stretching vibration absorption peak remains unaffected. These results indicate that the interaction between CS and the Fe^{3+}-treated quartz surface has weakened (Markovski et al., 2014; Wang et al., 2019). This phenomenon can be attributed to the formation of a small number of hydrophilic components, similar to iron hydroxide, on the quartz surface, which may have hindered the effective adsorption of dodecamine and CS.

The results presented in Fig. 8 demonstrate that after the interaction between magnetite, CS, and dodecamine, the intensity of the characteristic peak of CS in the infrared spectrum of magnetite weakens, indicating that a weak interaction has occurred on the surface of magnetite treated with CS and dodecamine. After the addition of Fe^{3+}, the absorption peak intensities at 3435.56 and 1631.89 cm^{-1} in the infrared spectrum of magnetite are strengthened, and significant changes occur on the surface of magnetite. A characteristic peak of $-CH_2-$ appears at 2929–2932 cm^{-1}, and an absorption peak appears in the range of 776–656 cm^{-1}, which is a characteristic peak of Fe–O on the surface of magnetite. These results indicate that Fe^{3+} is adsorbed to the magnetite surface in the form of iron hydroxide, resulting in the formation of hydrophilic groups similar to iron hydroxide on the magnetite surface. This may affect the interaction between the mineral surface and the reagent.

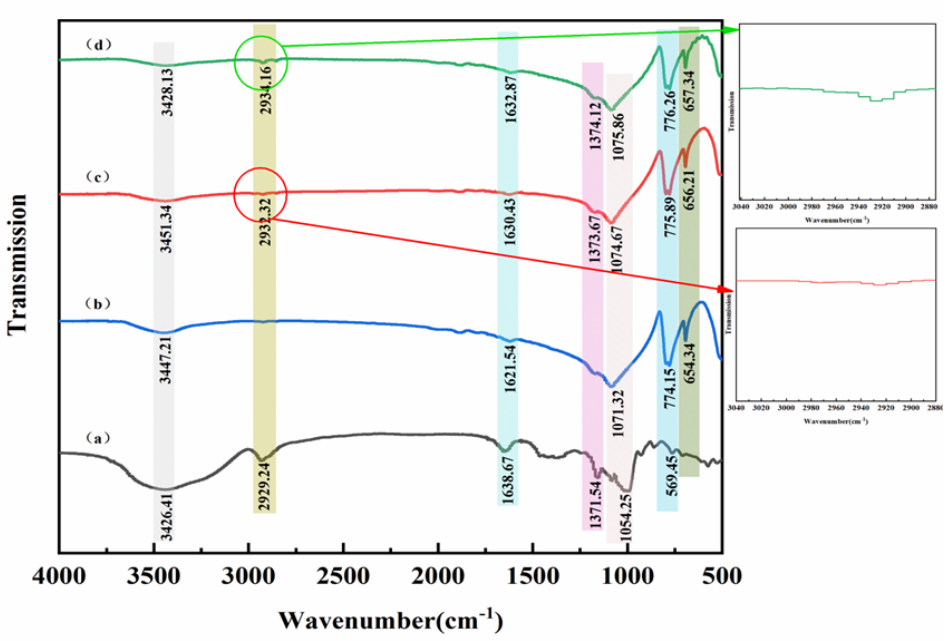

Fig. 7. FT-IR of (a) CS, (b) quartz, (c) quartz + CS + DDA, and (d) quartz + Fe^{3+} + CS + DDA

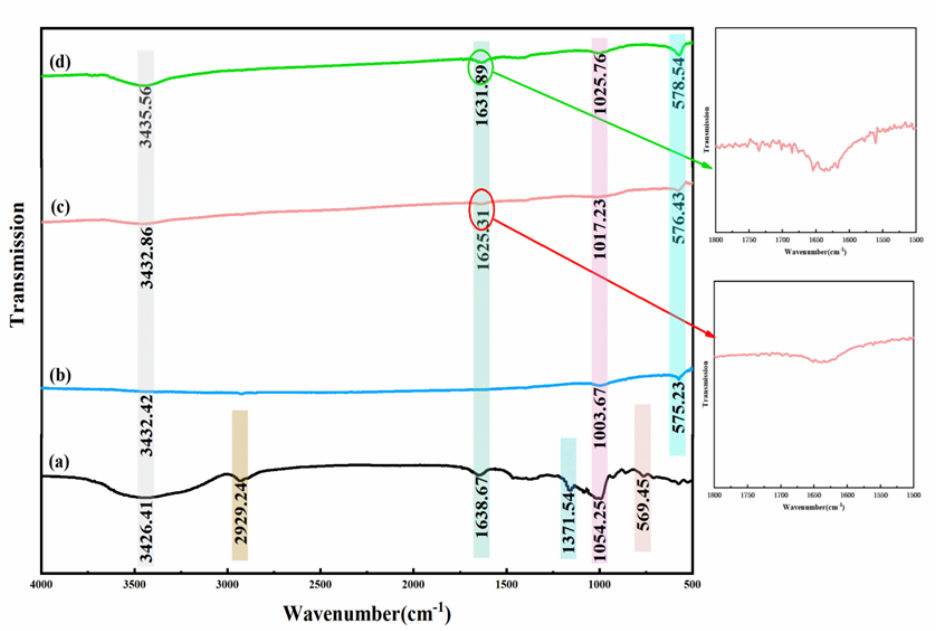

Fig. 8. FT-IR spectra of (a) CS, (b) magnetite, (c) magnetite + CS + DDA, and (d) magnetite + Fe^{3+} + CS + DDA

3.4. Zeta potential analysis

The results presented in Fig. 9 demonstrate the surface zeta potential properties of quartz under different pH conditions in different systems. The isoelectric point of quartz in deionized water was determined to be pH 1.6. However, after interacting with Fe^{3+}, its isoelectric point significantly increased to pH 7.6. Compared to its state in deionized water, the addition of Fe^{3+} caused a positive change in the zeta potential of the quartz surface, proving that the quartz surface has a high capacity for adsorbing Fe^{3+}. Through further analysis, we found that when CS was added to the Fe^{3+} pretreated quartz surface, the isoelectric point decreased to pH 1.3. The zeta potential of quartz + CS is more negative than that of quartz + Fe^{3+} + CS. At pH 10, the zeta potential of quartz + CS is approximately -45 mV, while that of quartz + Fe^{3+} + CS is approximately -42 mV. This indicates that the pre-adsorbed Fe^{3+} weakens the

effective adsorption of CS on quartz rather than enhancing it. This trend is also consistent with our FT-IR results for quartz, where the -CH_2- band associated with CS is weakened in the presence of Fe^{3+}. By analyzing the zeta potential, we came to the following conclusion: the interaction between CS and Fe^{3+} weakened the adsorption efficiency of CS on the quartz surface. This finding matches the results of the pure mineral flotation test, providing further evidence of the utility of zeta potential analysis in determining the properties of mineral surfaces and how they interact with different agents.

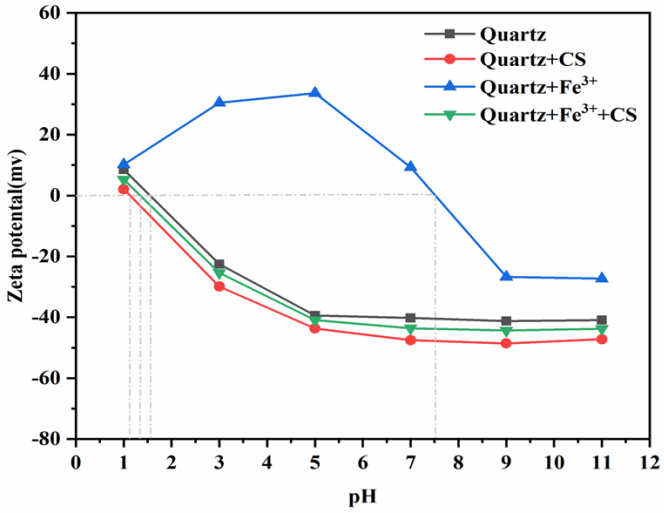

Fig. 9. Zeta potentials of quartz in solutions as a function of solution pH value

The results presented in Fig. 10 demonstrate the change in the zeta potential of CS on the surface of magnetite before and after Fe^{3+} treatment. In deionized water, the isoelectric point of magnetite is pH 6.1. After interacting with Fe^{3+}, the isoelectric point of magnetite significantly increases to pH 8.2. This change indicates that the addition of Fe^{3+} causes a significant change in the zeta potential of the magnetite surface compared to the untreated state. Thus, it can be inferred that the surface of magnetite is indeed have capability to adsorb Fe^{3+}. Through further analysis, we found that when CS was added to magnetite slurry pretreated with Fe^{3+}, the isoelectric point of the magnetite surface changed slightly to pH 6.7. As the pH value increased, the zeta potential of the magnetite surface also showed a slight shift in the positive direction. At the same time, on the surface of magnetite, Fe^{3+} hydrolysis products promote additional adsorption sites for CS, thereby enhancing the inhibitory effect. This trend revealed that CS could successfully adsorb onto the surface of magnetite treated with Fe^{3+}. The zeta potential study results demonstrate that the adsorption ability of magnetite for CS is increased in the presence of both Fe^{3+} and CS. This enhancement may prevent magnetite from floating.

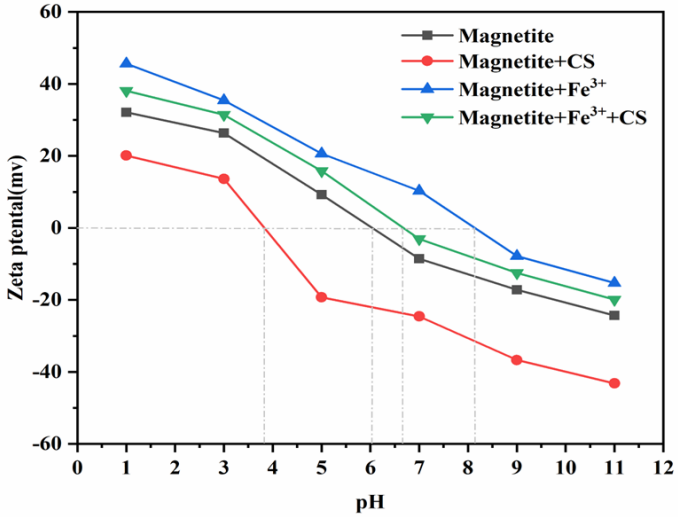

Fig. 10. Zeta potentials of magnetite in solutions as a function of solution pH value

3.5. Contact angle measurement

In order to study the effect of CS and Fe^{3+} as a combination depressant on the hydrophobic properties of magnetite and quartz surfaces, we introduced the concept of contact angle θ. The contact angle θ is the angle between the tangent of the wetting liquid and the solid surface at the point where the solid, liquid, and gas phases meet. The size of the angle is directly determined by the surface tension characteristics of the solid surface. The higher the contact angle θ, the lower the wettability cosθ of the mineral, indicating that the mineral surface is more hydrophobic (Kar et al., 2013). Conversely, the smaller the contact angle θ, the higher the wettability cosθ of the mineral, indicating that the mineral surface has stronger hydrophilicity (He et al., 2022). As shown in Fig. 11 and Fig. 12, in deionized water with a pH value of 10, the contact angle of quartz is 42.61°; in comparison, that of magnetite is 28.34°. The difference indicates that the two minerals exhibit different flotation characteristics in their natural state. Following treatment with dodecylamine, the contact angle of the quartz sample increased significantly to 67.34°; in comparison, that of the magnetite sample increased to 43.16°. The results indicate that quartz has stronger hydrophobicity than magnetite and is more easily selected during the flotation process (Meng et al., 2022). However, when quartz and magnetite were treated with CS and dodecylamine in combination, the contact angles decreased to 59.38° and 38.54°, respectively, accompanied by a significant weakening of flotation properties. Although the contact angles of minerals decreased, the extent of the decrease was relatively limited, indicating that the addition of CS did not completely change the hydrophobic properties of the mineral surfaces, which remained relatively weak. Through further analysis, we found that after Fe^{3+} treatment, the contact angles of quartz and magnetite were 55.13° and 30.21°, respectively. Compared with the addition of CS, the contact angle of quartz decreased by 4.25°, whereas that of magnetite decreased by 8.33°. The measurement and analysis of contact angles demonstrate that the addition of Fe^{3+} and CS has a significant effect on magnetite, inducing a decrease in the contact angle of magnetite and an increase in hydrophilicity, making it difficult to float.

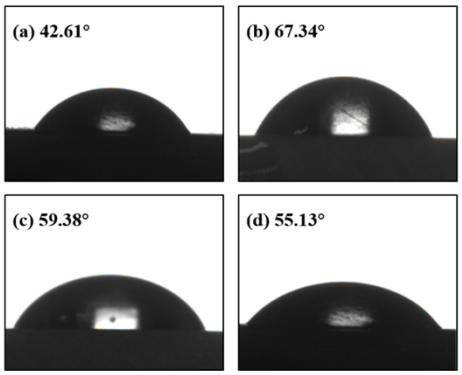

Fig. 11. Contact angle of the quartz surface under different conditions: (a) quartz; (b) quartz + 6mg/l DDA; (c) quartz + 8mg/l CS + 6mg/l DDA; (d) quartz + 150mg/l Fe^{3+} + 8mg/l CS + 6mg/l DDA

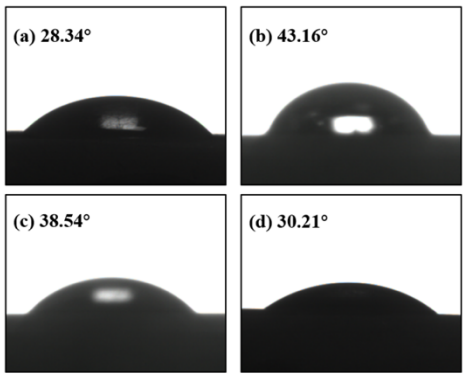

Fig. 12. Contact angle of the magnetite surface under different conditions: (a) magnetite; (b) magnetite + 6mg/l DDA; (c) magnetite + 8mg/l CS+ 6mg/l DDA; (d) magnetite +Fe^{3+} + 8mg/l CS + 6mg/l DDA

3.6. SEM analysis

SEM analysis of quartz and magnetite was conducted to compare the surface characteristics of the minerals after treatment with CS and CS/Fe^{3+}. As shown in Fig. 13, regardless of whether CS is used in isolation or in combination with Fe^{3+}, no significant changes in the starch adsorption characteristics on the quartz surface were found. Through further analysis, we found that following the addition of Fe^{3+}, a comparison of the mass percentages before and after treatment revealed that no iron elements were detected on the quartz surface, indicating that the adsorption effect of Fe^{3+} on the quartz surface was not efficient.

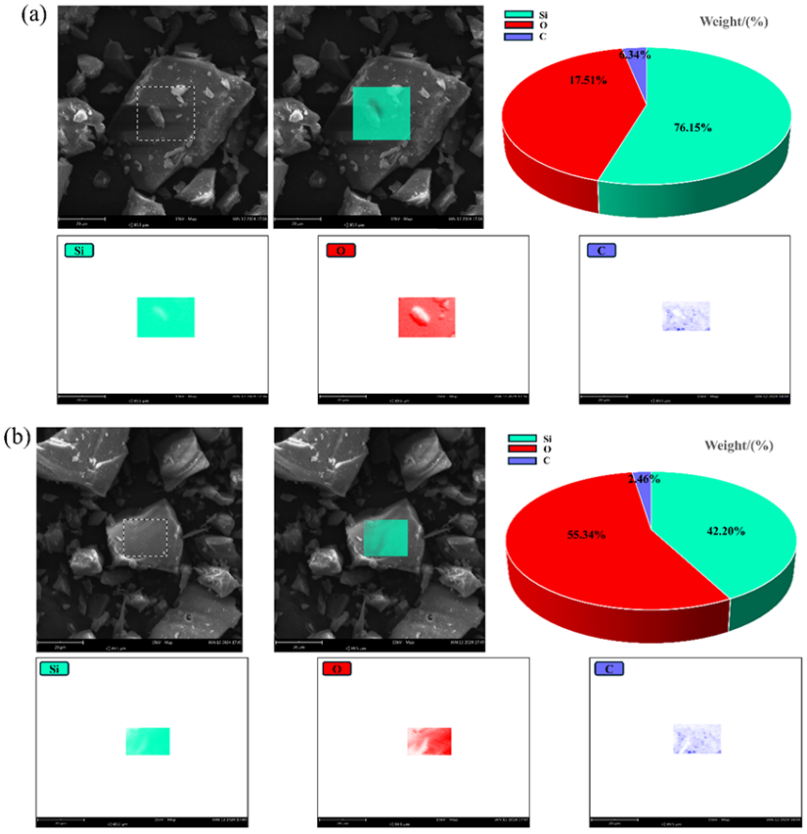

Fig. 13. SEM characteristics mapping of quartz with (a) CS, (b) CS, and Fe^{3+}

As shown in Fig. 14(a), when the CS depressant was used, the surface morphology of magnetite changed significantly, and its surface was covered with a layer of fine particles. The results presented in Fig. 14(b) further demonstrate that the adsorption ability of these fine particles is enhanced after the addition of Fe^{3+}, and their distribution density increases. This may be due to the presence of substances similar to iron hydroxide, such as $Fe(OH)_2$ and $Fe(OH)_3$, covering the surface of magnetite. The results presented in the mass percentage analysis graph demonstrate that the concentration of iron on the magnetite surface increased by 0.98%, from 75.17% to 76.15%. Based on these results, Fe^{3+} possesses a greater adsorption ability on the magnetite surface than quartz and yields more noteworthy outcomes.

3.7. Mechanism of adsorption

The results presented in Fig. 15 demonstrate the mechanism of action of CS and Fe^{3+} as a combined depressant in the flotation separation process of magnetite and quartz. CS adsorbs mineral surfaces through hydrogen bonding, which significantly enhances the hydrophilicity of the minerals. Through further analysis, we found that the addition of Fe^{3+} further enhanced the adsorption effect. The interaction between Fe^{3+} and starch molecules formed a more stable compound. The change not only optimized the adsorption performance of starch on the mineral surface but also further improved the hydrophilicity of the mineral surface, laying the foundation for the effective flotation separation of magnetite and quartz.

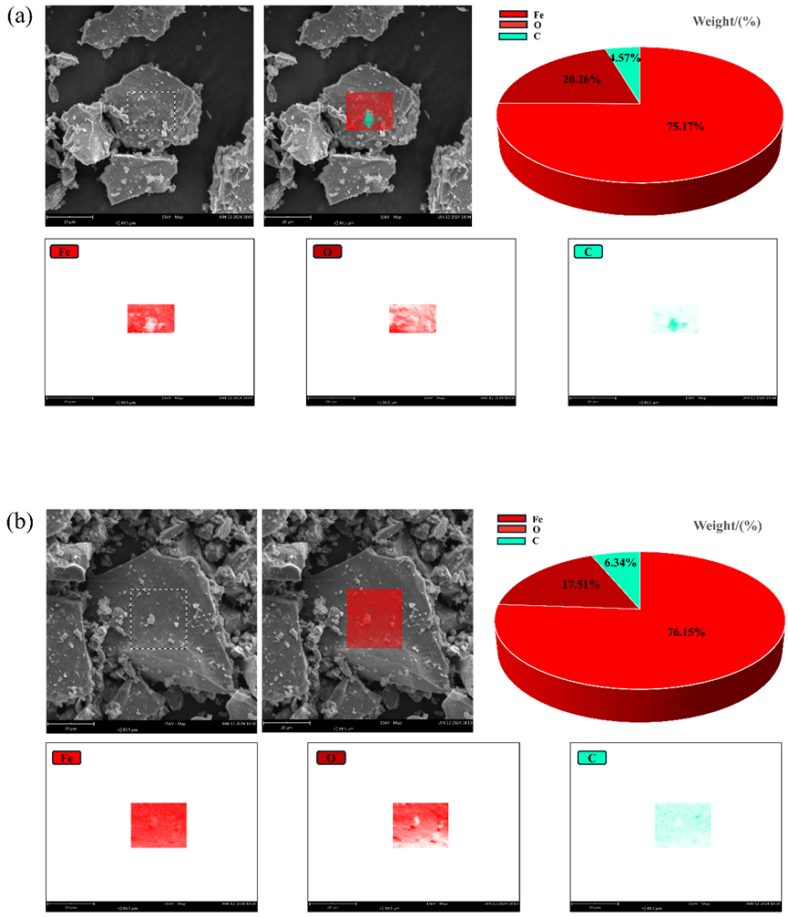

Fig. 14. SEM characteristics mapping of magnetite with (a) CS, (b) CS, and Fe^{3+}

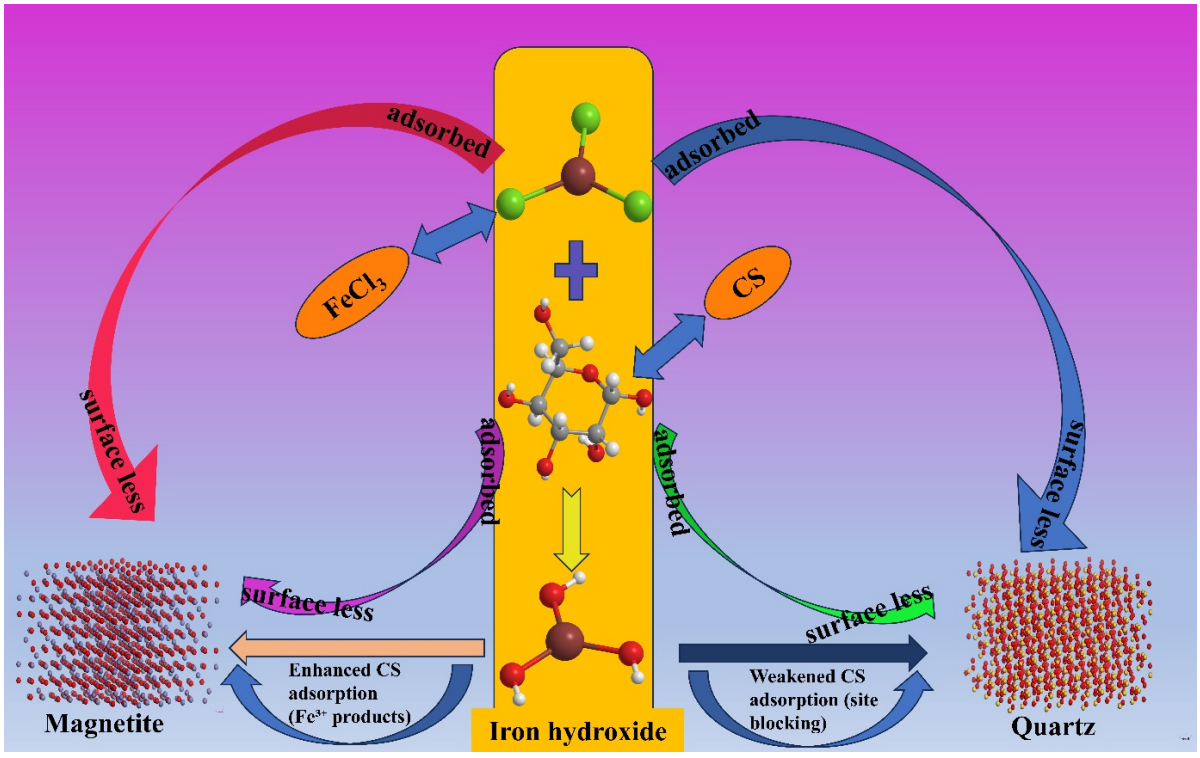

Fig. 15. Schematic representation of the adsorption interactions of magnetite and quartz through the combined use of CS and Fe^{3+}

4. Conclusions

The In this study, the effect of Fe^{3+} and CS as a combined depressant on the flotation separation of magnetite and quartz, in addition to their interaction mechanisms with mineral surfaces, were studied by using micro-flotation experiments, contact angle testing, solution chemistry calculations, Fourier transform infrared spectroscopy (FT-IR), zeta potential testing, and scanning electron microscopy (SEM). The results of the micro-flotation experiment indicate that the combined use of CS and Fe^{3+} has a significant effect on the flotation separation of magnetite and quartz. Under optimal flotation conditions, the recovery rate of magnetite decreased to 19.30%, while that of quartz reached up to 72.01%. This significant difference is attributed to the addition of Fe^{3+} to the slurry, which caused magnetite surfaces to adsorb more hydrophilic components (such as -OH groups), thereby effectively depressing the flotation process of magnetite. In addition, the adsorption force of CS and Fe^{3+} on the surface of magnetite is significantly greater than its adsorption force on the surface of quartz. The results of SEM analysis, solution chemistry calculations, and FT-IR analysis further indicate that after the addition of Fe^{3+}, precipitates such as $Fe(OH)_{2(s)}$ and $Fe(OH)_{3(s)}$ were formed in the solution. These precipitates covered the mineral surface, and the formation of $Fe(OH)_{3(s)}$ significantly reduced the hydrophobicity of the magnetite surface, thereby leading to a decrease in the magnetite recovery rate. Based on the results of contact angle analysis and zeta potential testing, the mineral surface displays zeta potential properties similar to those of iron oxide surfaces following the addition of metal ions such as Fe^{3+}, increasing the probability that magnetite would interact with starch. Concurrently, the hydroxyl iron compounds formed on the mineral surface not only cover the mineral surface but also make it more hydrophilic than the quartz surface, thereby further weakening the flotation effect of magnetite. The above results provide guidance and reference for a deeper understanding of the mechanism of action of the Fe^{3+} and CS combined depressant in the flotation separation of magnetite and quartz.

Acknowledgments

This work was supported by the National Natural Science Foundation of China under Grant 52174245, the Natural Science Foundation of Fujian Province under Grant 2021J01552, and the Open Foundation of the State Key Laboratory of Mineral Processing (Nos. BGRIMM-KJSKL-2021-02 and BGRIMM-KJSKL2022-03).

References

AN, H., MA, Q., ZHANG, F., ZHAI, C., SUN, J., TANG, Y., WANG, W., 2024. *Insight into microstructure evolution during starch retrogradation by infrared and Raman spectroscopy combined with two-dimensional correlation spectroscopy analysis*. Food. Hydrocolloids. 146, 109174.

AMMAR, M., EL-HALIM, A., SHARADA, H., FADEL, M., YEHIA, A., 2022. *Study on the interactions of two models of enzymes as eco-friendly depressants in flotation separation of apatite from hematite*. Appl. Surf. Sci. 601. 154223.

BENAVENTE, D., RUIZ, M., 2025. *García-Martínez,et al.Estimation of mineral saturation and CO_2 partial pressure in natural waters using electrical conductivity and pH: A fast and versatile on-site tool*. J. Hydrol. 660, 133474.

CAI, J., DENG, J., WANG, L., HU, M., XU, H., HOU, X., WU, B., LI, S., 2022. *Reagent types and action mechanisms in ilmenite flotation: A review*. Int. J. Min. Met. Mater. 29, 1656-69.

CHANG, L., JIUSHUAI, D., CHENQUAN, N., DONGHUI, W., KAI, X., LONGHUA, X., XI, Z., 2022. *Reverse froth flotation separation of limonite and quartz with cationic gemini surfactant*. Miner. Eng. 177, 107391.

CHEN, Q., TIAN, M., KASOMO, R. M., LI, H., ZHENG, H., SONG, S., LUO, H., HE, D., 2020. *Depression effect of Al(Ⅲ) and Fe(Ⅲ) on rutile flotation using dodecylamine polyxyethylene ether as collector*. Colloids. Surf. A. 603, 161617.

CHEN, Y., TONG, X., FENG, D., XIE, X., 2018. *Effect of Al (III) Ions on the Separation of Cassiterite and Clinochlore Through Reverse Flotation*. Minerals. 8, 347.

CHOI, J., CHOI, S. Q., PARK, K., HAN, Y., KIM, H., 2016. *Flotation behaviour of malachite in mono- and di-valent salt solutions using sodium oleate as a collector*. Int. J. Miner. Process. 146, 38-45.

DE SOUZA CORREA, A., MALENA FERNANDES LIMA, R., 2023. *Effect of dolomite on cationic reverse flotation of iron ore with amide-amine*. Miner. Eng. 201, 108226.

GAO, Z., JIANG, Z., SUN, W., GAO, Y., 2021. *Typical roles of metal ions in mineral flotation: A review*. Trans. Nonferrous. Met. Soc. China. 31, 2081-101.

GAO, Z., WANG, C., SUN, W., GAO, Y., KOWALCZUK, B., 2021. *Froth flotation of fluorite: A review*. Adv. Colloid. Interface. Sci. 290, 102382.

GUANG, H., SHUMING, W., HAN, W., QICHENG, C., 2019. *Effect of starch on surface properties of pyrite and chalcopyrite and its response to flotation separation at low alkalinity*. Miner. Eng. 143, 106015-106015.

HE, J., CHEN, H., ZHANG, M., CHEN, L., YAO, Q., DAI, Y., ZHU, L., LIU, C., 2022. *Combined depressants of Ferric chloride, Cu^{2+} or Al^{3+} and sodium silicate on the flotation of fluorite and quartz*. Colloids. Surf. A. 643, 128702.

HENRY, N., N., SENOZAN., 2001. *The Henderson-Hasselbalch Equation: Its History and Limitations*. J. Chem. Educ. 80, 146.

HONG, G., MWEENE, L., 2025. *Surface chemical properties of goethite with nickel and cobalt in high alkaline environment: experimental and theoretical study*. Colloid Surf. Physicochem. Eng. Asp. 709, 136164.

JIE, Z., WEIQING, W., JING, L., YANG, H., QIMING, F., HONG, Z., 2014. *Fe(III) as an activator for the flotation of spodumene, albite, and quartz minerals*. Miner. Eng. 61, 16-22.

KAR, B., SAHOO, H., RATH, S. S., DAS, B., 2013. *Investigations on different starches as depressants for iron ore flotation*. Miner. Eng. 49, 1-6.

LI, C., BAI, S., DING, Z., YU, P., WEN, S., 2019. *Visual MINTEQ model, ToF–SIMS, and XPS study of smithsonite surface sulfidation behavior: Zinc sulfide precipitation adsorption*. J. Taiwan. Inst. Chem. Eng. 96, 53-62.

LI, Y., QUANJUN, L., SHIMEI, L., CHAO, S., YANG, G., JIANWEN, S., 2019. *The synergetic depression effect of KMnO4 and CMC on the depression of galena flotation*. Chem. Eng. Commun. 206, 581-91.

LIU, Q., LI, Y., ZHANG, J., CHI, Y., RUAN, X., LIU, J., QIAN, G., 2011. *Effective removal of zinc from aqueous solution by hydrocalumite*. Chem. Eng. J. 175, 33-8.

LUO, L., WU, H., XU, L., MENG, J., LU, J., ZHOU, H., HUO, X., HUANG, L., 2021. *An in-situ ATR-FTIR study of mixed collectors BHA/DDA adsorption in ilmenite-titanaugite flotation system*. Int. J. Min. Sci. Technol. 31, 689-97.

LUO, L., ZHANG, Y., BAO, S., CHEN, T., 2016. *Utilization of Iron Ore Tailings as Raw Material for Portland Cement Clinker Production*. Adv. Mater. Sci. Eng. 2016, 1-6.

MARKOVSKI, J. S., MARKOVIĆ, D. D., ĐOKIĆ, V. R., MITRIĆ, M., RISTIĆ, M. Đ., ONJIA, A. E., MARINKOVIĆ, A. D., 2014. *Arsenate adsorption on waste eggshell modified by goethite, a-MnO_2 and goethite/a-MnO_2*. Chem. Eng. J. 237, 430-42.

MENG, J., XU, L., WANG, D., XUE, K., LUO, L., SHI, X., 2022. *The activation mechanism of metal ions on spodumene flotation from the perspective of in situ ATR-FTIR and ToF-SIMS*. Miner. Eng. 182, 107567.

OULKHIR, A., LYAMLOULI, K., ELFAHMY, H., 2025. *Remarkable Effect of Sugar Waste Pyrolysis Oil as a Calcite Collector for Enhanced Phosphate Beneficiation via Reverse Flotation*. ACS. Sustainable. Chem. Eng. 0520, 6706-6719.

OULKHIR, A., LYAMLOULI, K., OUSSFAN, A. ORANGE, F., ETAHIRI, A., BENHIDA, R., 2025. *Efficient flotation separation approach of apatite from calcite for phosphate up-grading using phosphorylated starch macromolecules as a selective depressant*. Carbohydr. Polym. 348, 122878.

QIU, X., YANG, H., CHEN, G., LUO, W., 2018. *An Alternative Depressant of Chalcopyrite in Cu–Mo Differential Flotation and Its Interaction Mechanism*. Minerals. 9, 1-1.

RATH, S., SAHOO, H., 2022. *A Review on the Application of Starch as Depressant in Iron Ore Flotation. Miner. Process*. Extr. Metall. Rev. 43, 122-35.

ROCHA, M., MACHADO, S., PEREIRA, A., 2019. *Effect of ground corn and cassava flour on the flotation of iron ore tailings*. J. Mater. Res. Technol-JMRT. 8, 1510-4.

RUAN, Y., ZHANG, Z., LUO, H., XIAO, C., ZHOU, F., CHI, R., 2018. *Effects of Metal Ions on the Flotation of Apatite, Dolomite and Quartz*. Minerals. 8, 141.

SHEN, L., SUN, N., XU, R., SUN, W., WANG, L., 2023. *Adsorption mechanisms of activated surface of quartz and feldspar with mixed NaOL/DDA*. Sep. Purif. Technol. 314, 123501.

TANG, M., TONG, X., 2020. *The relationship between anion distribution in process water and flotation properties of iron oxides*. Miner. Eng. 154, 106378.

TANG, M., WEN, S., 2019. *Effects of Cations/Anions in Recycled Tailing Water on Cationic Reverse Flotation of Iron Oxides*. Minerals. 9, 161.

WANG, C., LIU, R., SUN, W., JING, N., XIE, F., HE, Q. Z. D., 2021. *Selective depressive effect of pectin on sphalerite flotation and its mechanisms of adsorption onto galena and sphalerite surfaces*. Miner. Eng. 170, 106989.

WANG, G., LIU, J., XU, L., QUAN, Y., YU, J., 2023. *Geochronology (U-Pb and Re-Os) and H O S isotopes reveal ore fluid origin and crucial role of meteoric water for Laozuoshan quartz-vein-hosted gold metallogeny in Jiamusi, NE China*. Ore. Geol. Rev. 153, 105267.

WANG, X., ZHANG, Y., LIU, T., CAI, Z., 2019. *Influence of metal ions on muscovite and calcite flotation: With respect to the pre-treatment of vanadium bearing stone coal*. Colloids. Surf. A. 2019, 564, 89-94.

WENBO, L., SHAOKAI, C., LIBO, Z., YUEXIN, H., 2023. *Enhanced iron recovery from magnetic separation of ultrafine specularite through polymer-bridging flocculation: A study of flocculation performance and mechanism*. Sep. Purif. Technol. 308, 122882.

YANG, S., WANG, L., 2018. *Structural and functional insights into starches as depressant for hematite flotation*. Miner. Eng. 124, 149-57.

YANG, S., WANG, L., 2019. *Measurement of froth zone and collection zone recoveries with various starch depressants in anionic flotation of hematite and quartz*. Miner. Eng. 138, 31-42.

YEHIA, A., ABD EL-HALIM, S., SHARADA, H., FADEL, M., AMMAR, M., 2021. *Application of a fungal cellulase as a green depressant of hematite in the reverse anionic flotation of a high-phosphorus iron ore*. Miner. Eng. 167, 106903.

YUAN, J., ZHANG, Y., YU, A., WEN, S., BAI, S., 2025. *Flotation separation of ilmenite and titanaugite modified by Fe^{2+}-assisted peroxymonosulfate oxidation: Performance and activation mechanism*. Appl. Surf. Sci. 682.

ZHAN, D., JIE, L., JIAQIAO, Y., ANMEI, Y., SHUNMING, W., SHAOJUN, B., 2023. *Insights into the influence of calcium ions on the adsorption behavior of sodium oleate and its response to flotation of quartz: FT-IR, XPS and AMF studies*. Miner. Eng. 204, 108437.

ZHAN, C., YAHUI, Z., YONGDAN, C., 2013. Reverse Flotation of Quartz From Magnetite Ore with Modified Sodium Oleate. Miner. Process. Extr. 34, 320-330.

ZHANG, X., ZHU, Y., XIE, Y., SHANG, Y., ZHENG, G., 2017. *A novel macromolecular depressant for reverse flotation: Synthesis and depressing mechanism in the separation of hematite and quartz*. Sep. Purif. Technol. 186, 175-81.

ZHAO, C., SUN, C., YIN, W., LUO, B., 2019. *An investigation of the mechanism of using iron chelate as a collector during scheelite flotation*. Miner. Eng. 131, 146-53.